Electronic Supplementary Information

for

Direct and Remote Control on Electronic Structures and Redox Potentials in μ-Oxo Diferric Complexes

Sebastian Finke, Anja Stammler, Jan Oldengott, Stephan Walleck, and Thorsten Glaser*,

Lehrstuhl für Anorganische Chemie I, Fakultät für Chemie, Universität Bielefeld,Universitätsstr. 25, D-33615 Bielefeld, Germany

** To whom correspondence should be addressed. E-mail: thorsten.glaser@unibielefeld.de (T.G.)*

Table S1. Crystal data and refinement parameters.

	[(susan^{OMe})FeCl(μ-O)FeCl](ClO$_4$)$_2$	[(susan^{OMe})Fe(OAc)(μ-O)Fe(OAc)](ClO$_4$)$_2$•MeCN	[(susan^{OMe})Fe(μ-O)(μ-OAc)Fe](ClO$_4$)$_3$•2MeCN	[(susan^{OMe})Fe(OH)(μ-O)Fe(OH)](ClO$_4$)$_2$•2C$_3$H$_7$OH	[(susan^{OMe})Fe(OAc)$_{0.8}$(HCOO)$_{0.2}$(μ-O)Fe(OH)](ClO$_4$)$_2$•C$_3$H$_6$O
Empirical formula	$C_{44}H_{66}Cl_4Fe_2N_8O_{13}$	$C_{50}H_{75}Cl_2Fe_2N_9O_{17}$	$C_{50}H_{75}Cl_3Fe_2N_{10}O_{19}$	$C_{50}H_{84}Cl_2Fe_2N_8O_{17}$	$C_{48.8}H_{75.6}Cl_2Fe_2N_8O_{17}$
Formula weight	1168.54	1256.79	1338.25	1251.85	1229.18
Crystal system	triclinic	monoclinic	triclinic	monoclinic	monoclinic
Space group	$P\bar{1}$	$P2_1/c$	$P\bar{1}$	$C2/c$	$P2_1/c$
a [Å]	14.7196(5)	19.5346(8)	11.7251(4)	25.2522(9)	13.2834(7)
b [Å]	14.9845(5)	13.2801(6)	13.1324(5)	15.5311(5)	15.3781(6)
c [Å]	15.0801(5)	22.9179(11)	20.1201(7)	16.9805(5)	28.2323(14)
α [°]	106.420(2)	90	80.277(2)	90	90
β [°]	110.555(2)	103.358(2)	77.367(2)	118.7610(10)	102.469(2)
γ [°]	110.926(2)	90	87.802(2)	90	90
V [Å^3]	2572.90(16)	5784.5(5)	2979.64(19)	5838.1(3)	5631.1(5)
Z	2	4	2	4	4
ρ [g cm^{-3}]	1.508	1.443	1.492	1.424	1.450
μ [mm^{-1}]	7.019	0.670	5.824	5.453	5.645
F(000)	1220.0	2640.0	1400.0	2648.0	2586.0
Crystal size [mm^3]	0.14 × 0.13 × 0.04	0.29 × 0.19 × 0.08	0.32 × 0.25 × 0.08	0.31 × 0.14 × 0.13	0.23 × 0.11 × 0.04
Radiation	CuKα (λ = 1.54178 Å)	MoKα (λ = 0.71073 Å)	CuKα (λ = 1.54178Å)	CuKα (λ = 1.54178 Å)	CuKα (λ = 1.54178 Å)
2Θ range [°]	7.08 to 137.53	2.14 to 60.07	4.56 to 136.73°	6.95 to 138.69	6.41 to 136.66
hkl ranges	-17 ≤ h ≤ 17 -17 ≤ k ≤ 18 -18 ≤ l ≤ 18	-27 ≤ h ≤ 27 -18 ≤ k ≤ 18 -32 ≤ l ≤ 32	-14 ≤ h ≤ 14 -15 ≤ k ≤ 15 -24 ≤ l ≤ 24	-30 ≤ h ≤ 30 -18 ≤ k ≤ 18 -20 ≤ l ≤ 20	-13 ≤ h ≤ 15 -18 ≤ k ≤ 18 -34 ≤ l ≤ 32
Collected refl.	39569	171985	47373	51018	57750
Unique refl., R_{int}	9173, 0.0698	16942, 0.0513	10879, 0.0347	5427, 0.0324	10277, 0.0432
Observed refl.($I > 2\sigma(I)$)	7387	12831	10392	5297	9269
Completeness	0.963	1.000	0.995	0.995	0.994
Data/restraints/param.	9173/176/737	16942/0/779	10879/4/759	5427/305/467	10277/1/744
Goodness-of-fit on F^2	1.021	1.026	1.030	1.033	1.021
R_1, wR_2 ($I > 2\sigma(I)$)	0.0419, 0.0964	0.0373, 0.0890	0.0485, 0.1324	0.0293, 0.0801	0.0333, 0.0839
R_1, wR_2 (all data)	0.0578, 0.1038	0.0605, 0.1001	0.0502, 0.1340	0.0298, 0.0806	0.0383, 0.0870
Largest peak/hole [e Å^{-3}]	0.35/-0.39	0.81/-0.38	0.91/-0.73	0.41/-0.30	0.68/-0.32
CCDC numbers	2289367	2289371	2289370	2289368	2289369

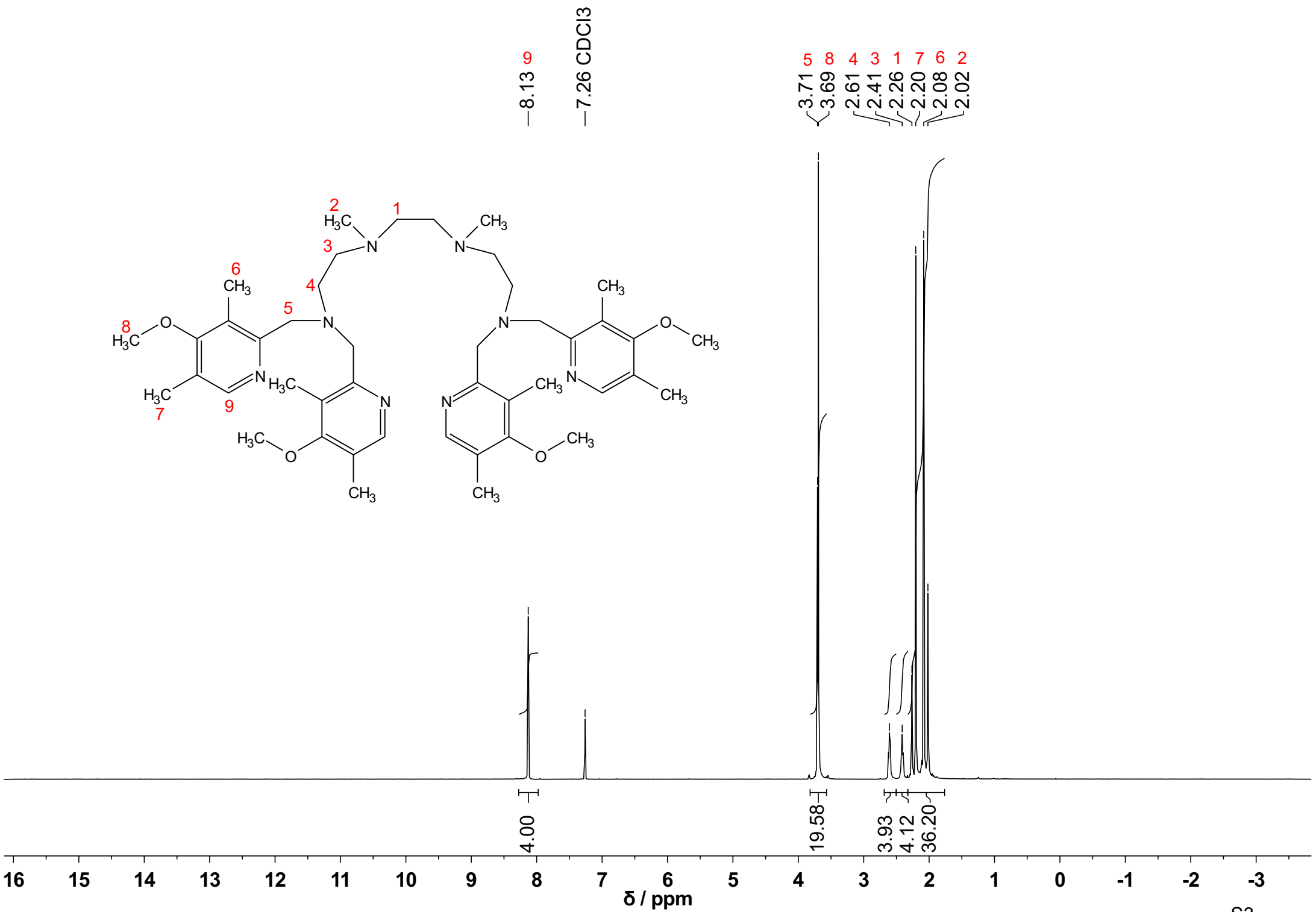

Figure S1. ^{1}H and ^{13}C NMR spectra of susan^{OMe}.

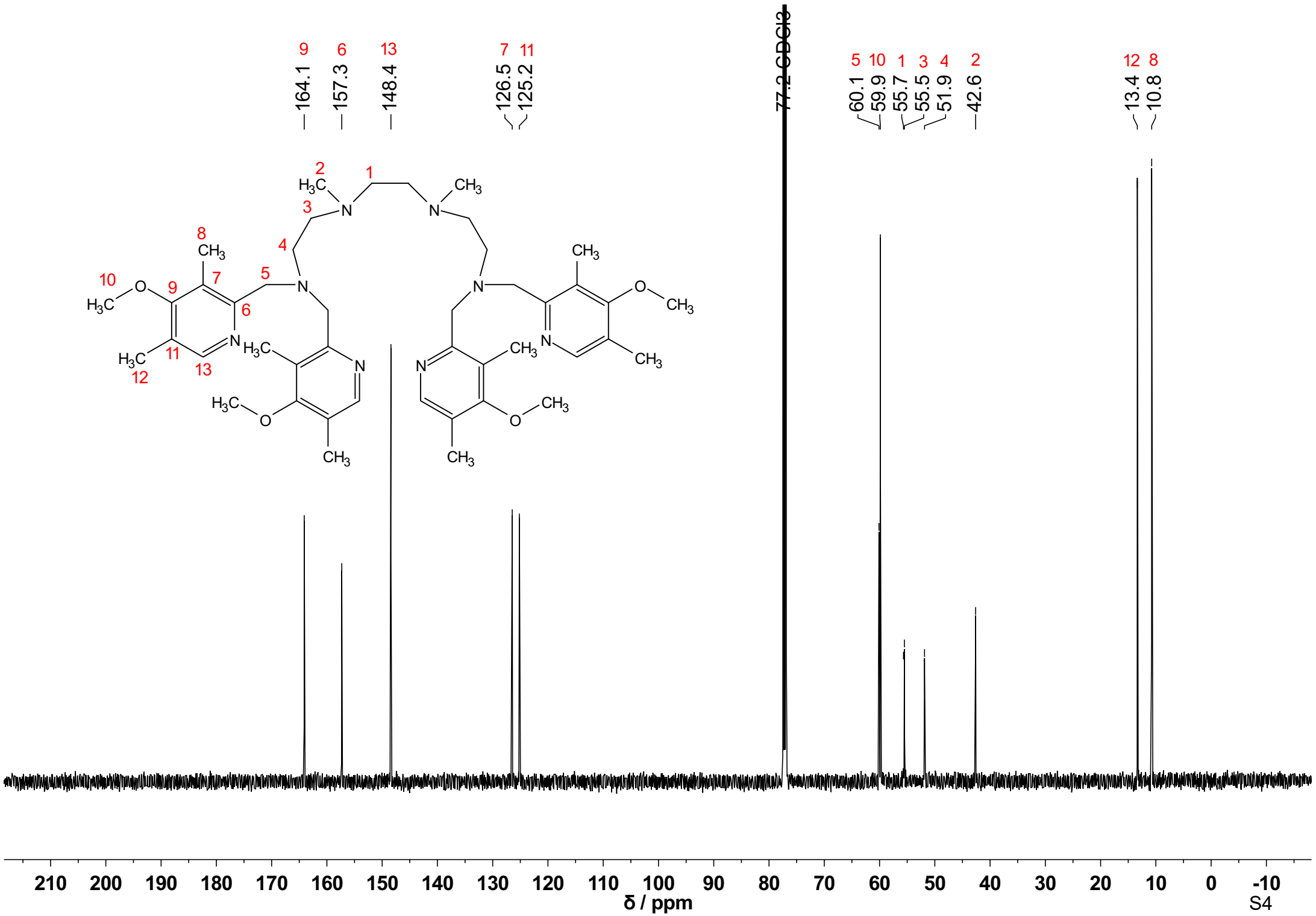
9 6 13 7 11
164.1
157.3
148.4
126.5
125.2
77.2 CDCl3
5 10 1 3 4 2
60.1
59.9
55.7
55.5
51.9
42.6
12 8
13.4
10.8
210 200 190 180 170 160 150 140 130 120 110 100 90 80 70 60 50 40 30 20 10 0 -10
δ / ppm

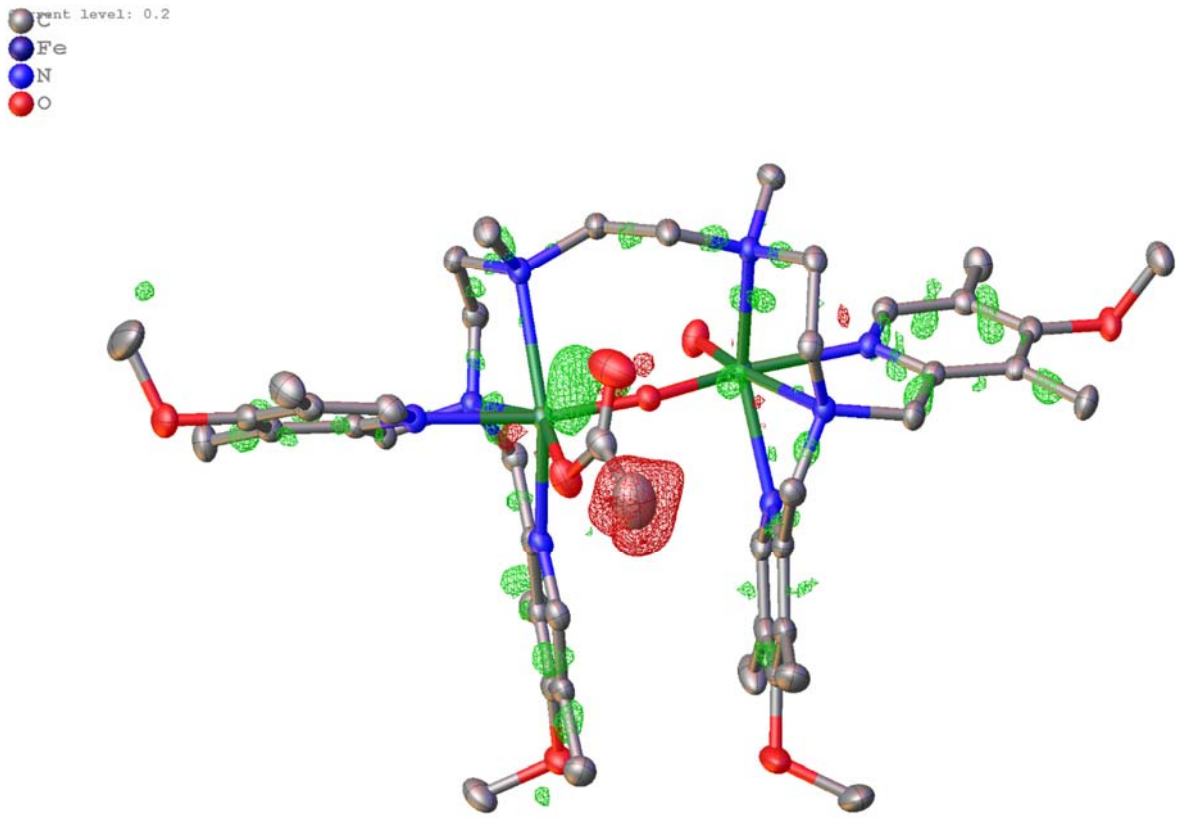

Figure S2. Thermal ellipsoide plot including residual electron density map at 0.2 e^-/Å level, positive residual density green, negative red. The map was calculated for a model with a fully occupied acetate position. The negative e^--density was finally better described as an approximately 0.8/0.2 acetate/formiate mixture in crystals of $[(susan^{OMe})Fe(OAc)_{0.8}(HCOO)_{0.2}(\mu\text{-}O)Fe(OH)](ClO_4)_2$•acetone.

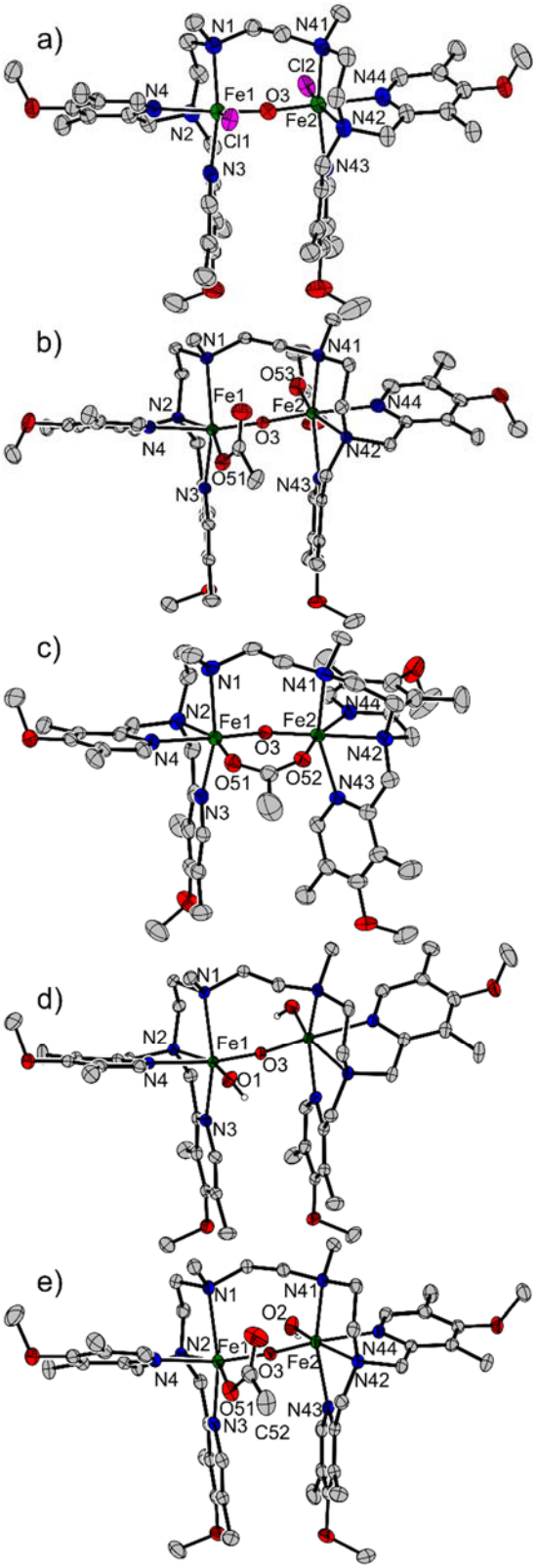

Figure S3. Thermal ellipsoid plots of a) $[(susan^{OMe})\{Fe^{III}Cl(\mu\text{-}O)Fe^{III}Cl\}]^{2+}$ in single-crystals of $[(susan^{OMe})\{Fe^{III}Cl(\mu\text{-}O)Fe^{III}Cl\}](ClO_4)_2$, b) $[(susan^{OMe})\{Fe^{III}(OAc)(\mu\text{-}O)Fe^{III}(OAc)\}]^{2+}$ in single-crystals of $[(susan^{OMe})\{Fe^{III}(OAc)(\mu\text{-}O)Fe^{III}(OAc)\}](ClO_4)_2\bullet CH_3CN$, c) $[(susan^{OMe})\{Fe^{III}(\mu\text{-}O)(\mu\text{-}OAc)Fe^{III}\}]^{3+}$ in single-crystals of $[(susan^{OMe})\{Fe^{III}(\mu\text{-}O)(\mu\text{-}OAc)Fe^{III}\}](ClO_4)_3\bullet 2CH_3CN$, d) $[(susan^{OMe})\{Fe^{III}(OH)(\mu\text{-}O)Fe^{III}(OH)\}]^{2+}$ in single-crystals of $[(susan^{OMe})\{Fe^{III}(OH)(\mu\text{-}O)Fe^{III}(OH)\}](ClO_4)_2\bullet 2i\text{-}PrOH$, and e) $[(susan^{OMe})\{Fe^{III}(OH)(\mu\text{-}O)Fe^{III}(OAc)\}]^{2+}$ in single-crystals of $[(susan^{OMe})\{Fe^{III}(OH)(\mu\text{-}O)Fe^{III}(OAc)\}](ClO_4)_2\bullet$acetone.

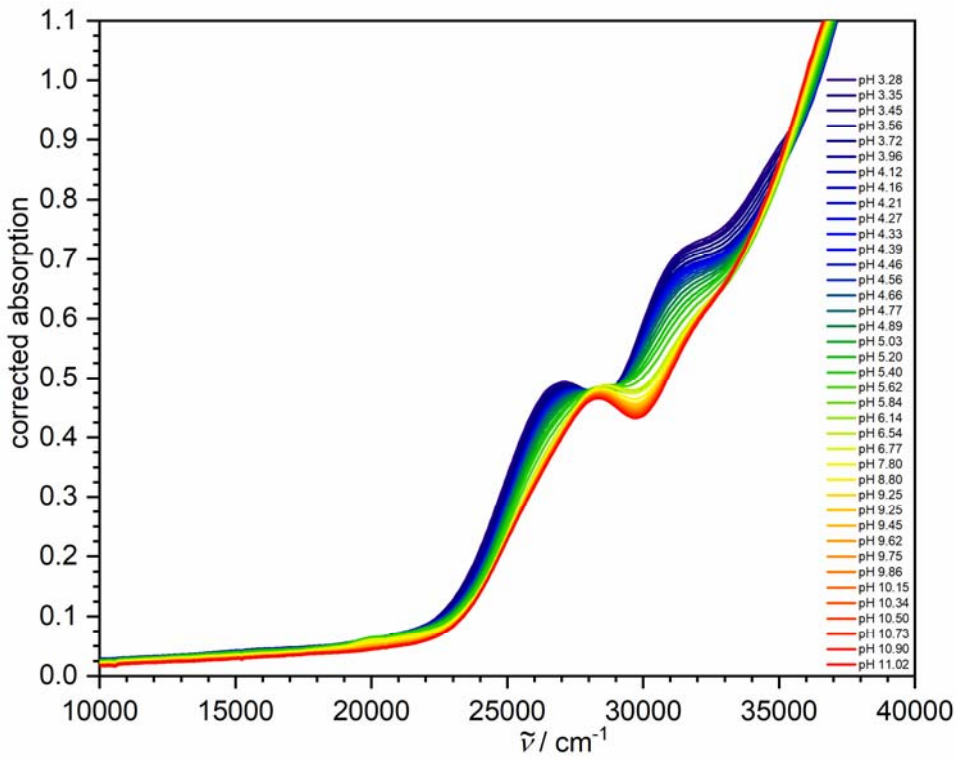

Figure S4. UV-Vis spectral changes observed for aqueous solutions of [(susan^{OMe}){Fe^{III}(OH)(μ-O)Fe^{III}(OH)}](ClO$_4$)$_2$ (c = 0.07 mM in 0.01 M NaClO$_4$ / HClO$_4$) in the pH-range 3.28-11.02.

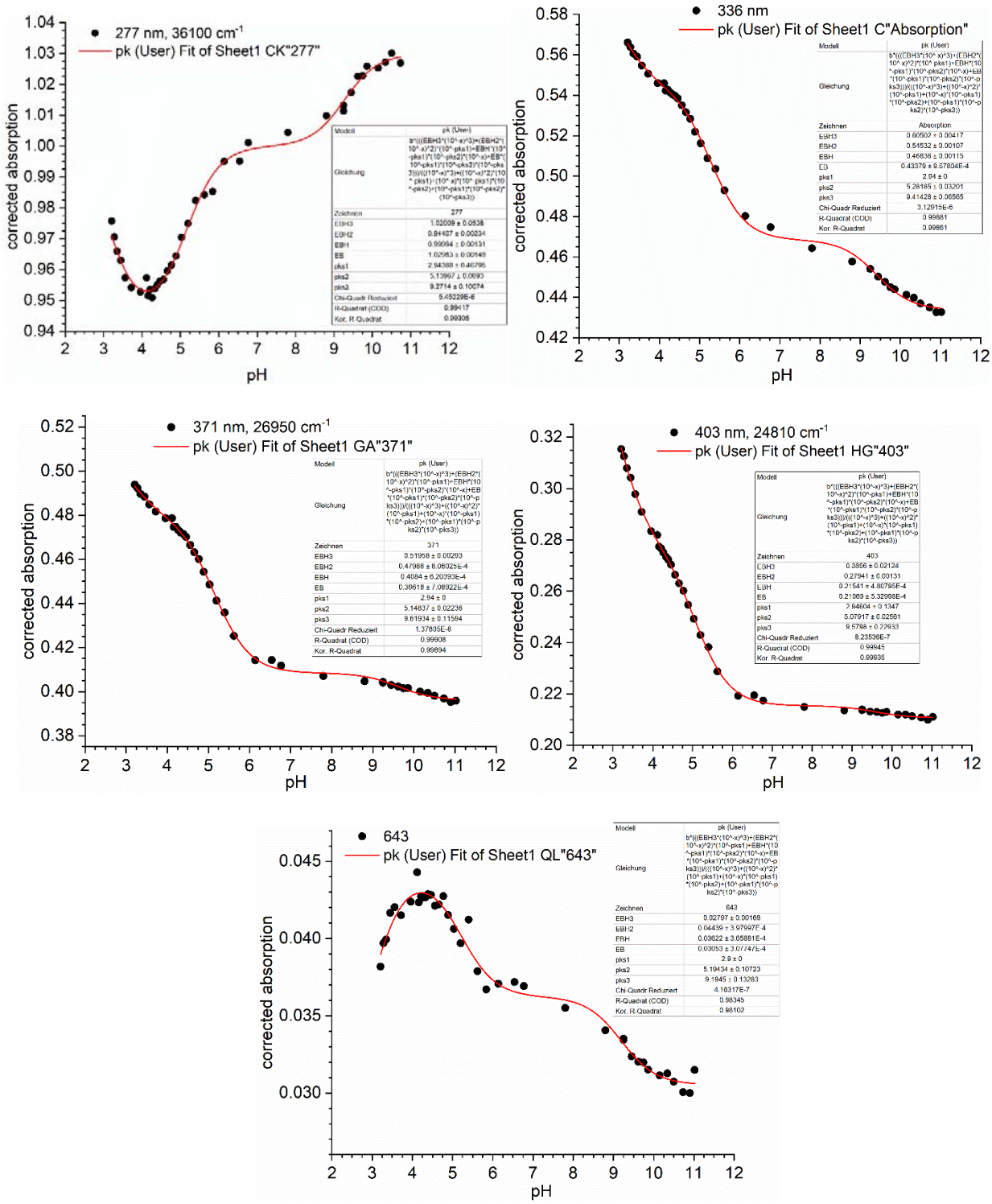

Figure S5. pH-Dependence of the corrected absorption at selected energies. Solid lines are fits to the equation for three protonation steps with $\Delta pK_S \leq 3$. For experimental conditions see Figure S4.